Impact of energetic particle driven geodesic acoustic modes on turbulence

D Zarzoso,[1, a)] Y Sarazin,[1] X Garbet,[1] R Dumont,[1] A Strugarek,[2, 1] J Abiteboul,[1] T Cartier-Michaud,[1] G Dif-Pradalier,[1] Ph Ghendrih,[1] V Grandgirard,[1] G Latu,[1] C Passeron,[1] and O Thomine[1]

[1)] *CEA, IRFM, F-13108 Saint-Paul-lez-Durance, France.*

[2)] *Laboratoire AIM Paris-Saclay, CEA/Irfu Université Paris-Diderot CNRS/INSU, 91191 Gif-sur-Yvette, France*

(Dated: 8 February 2013)

The impact on turbulent transport of geodesic acoustic modes excited by energetic particles is evidenced for the first time in flux-driven 5D gyrokinetic simulations using the GYSELA code. Energetic geodesic acoustic modes (EGAMs) are excited in a regime with a transport barrier in the outer radial region. The interaction between EGAMs and turbulence is such that turbulent transport can be enhanced in the presence of EGAMs, with the subsequent destruction of the transport barrier. This scenario could be particularly critical in those plasmas, such as burning plasmas, exhibiting a rich population of suprathermal particles capable of exciting energetic modes.

Understanding turbulent transport is crucial in numerous plasma physics frameworks, ranging from plasma laboratories such as nuclear fusion devices[1] to astrophysical systems such as the solar tachocline[2] or the atmospheres[3]. In this letter, we focus on the turbulent transport in toroidal nuclear fusion devices (tokamaks), where accurate predictions are essential on the route towards the steady-state production of energy. Together with turbulence, energetic particles (EPs) constitute a ubiquitous component of current and future tokamaks, due to both nuclear reactions and heating systems. EPs are characterized by energies larger than the thermal energy. Whereas the impact of turbulence on EP transport has been analyzed and found to be weak[4], the effect of EPs on turbulence has not been much studied so far (see e.g. Ref. 5) and represents the aim of our study. This analysis is done *via* the excitation by EPs of a class of modes naturally existing in tokamaks: the geodesic acoustic modes (GAMs)[6], which are the oscillatory component of large scale $E \times B$ zonal flows. The EP-driven GAMs are called EGAMs. These modes have been predicted theoretically[7,8], observed experimentally[9,10] and reported very recently numerically in the absence of turbulence[11] in gyrokinetic simulations with the 5D GYSELA code[12]. The motivation of the present work relies upon fluid simulations where the turbulence level was controlled by GAMs in the core/edge transitional regime[13]. In addition, experimental evidence of the role of GAMs in the edge-turbulence suppression has been reported for the first time during the analysis of the L-H transition in the ASDEX Upgrade tokamak[14]. However, in the context of core-turbulence suppression, the role of GAMs is less evident for several reasons. First, these modes are Landau damped in the core plasma. Second, since they are nonlinearly generated by turbulence, their external control has proven difficult. Last, their frequency ω_{GAM} is close to the characteristic turbulence frequency ω_{turb}, which means that the shearing rate provided by GAMs might be large compared to the autocorrelation time. In that respect, theoretical predictions of the shearing effect provided by GAMs are not straightforward. The first two difficulties are overcome in this letter by the presence of EPs providing a continuous excitation of the mode. The possibility to efficiently excite EGAMs in (global) flux-driven gyrokinetic simulations opens the way to the analysis of turbulence regulation by external ways as well as the impact of EPs on turbulence and sheds light on the third above-mentioned difficulty. In this letter, we provide first numerical evidence of the excitation of EGAMs in a fully developed ion temperature gradient (ITG) turbulence as well as the impact of these EGAMs on the turbulent transport. This is done by a source specifically designed to increase the population of EPs. Three main results are presented: (1) EGAMs can be excited in the presence of ITG turbulence in a steady-state regime, (2) the resulting oscillating radial electric shear is not able to suppress the core turbulence, on the contrary (3) a complex interaction between EGAMs and turbulence is evidenced, leading to a radial propagation of turbulence and the destruction of an existing transport barrier. These results are illustrated in figure 1, where we display the dependence on time and minor radius of the turbulent diffusivity governed by fluctuations of the radial $E \times B$ drift velocity v_{Er}. Three phases are clearly visible, and will be detailed in the remainder of this letter: (A) the energetic particle source is applied to a statistical steady-state turbulence regime, (B) a transport barrier is triggered and (C) EGAMs and turbulence coexist and interact with each other.

GYSELA solves the standard gyrokinetic equation in the electrostatic limit for the ion guiding-center distribution function in a simplified magnetic topology consisting of toroidal flux surfaces with circular poloidal cross-sections. In this model, the electrons are considered adiabatic. The self-consistent system is composed by the gyrokinetic equation coupled to the quasi-neutrality condition, providing the ion guiding-center distribution func-

---

[a)]Electronic mail: david.zarzoso-fernandez@polytechnique.org; Current address: Max-Planck-Institut für Plasmaphysik, EU-RATOM Association, Boltzmannstr. 2, Garching D-85748, Germany
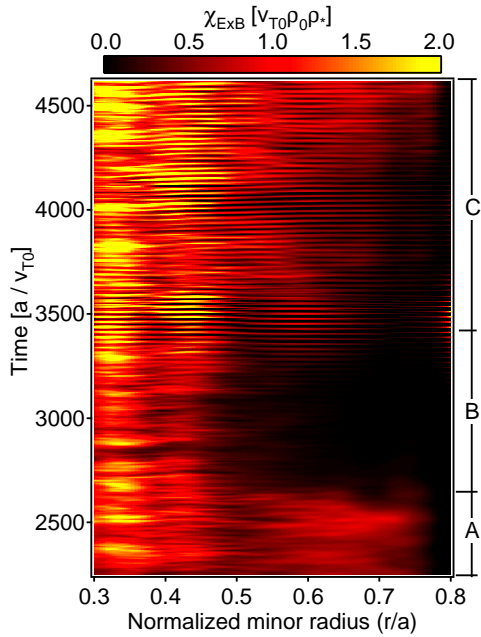
FIG. 1: Colormap of the $E \times B$ diffusivity ($\chi_{E \times B}$) with the three phases analyzed in the paper.

tion F and the electrostatic potential ϕ:

$$\frac{\partial F}{\partial t} + \mathbf{v} \cdot \boldsymbol{\nabla} F + \dot{v}_\parallel \frac{\partial F}{\partial v_\parallel} = \mathcal{C}(F) + S \qquad (1)$$

$$\phi - \langle \phi \rangle - \frac{1}{n_{\text{eq}}} \boldsymbol{\nabla}_\perp \cdot \left(\frac{n_{\text{eq}}}{B^2} \boldsymbol{\nabla}_\perp \phi \right) = \frac{n_i - n_{\text{eq}}}{n_{\text{eq}}} \qquad (2)$$

In eqs.(1-2) and hereafter, all quantities are normalized. Three normalizing (constant) quantities only are needed, namely density n_0, temperature T_0 and the magnetic field on the magnetic axis B_0. In this framework, temperatures are normalized to T_0, velocities are normalized to the thermal velocity $v_{T0} = (T_0/m_i)^{1/2}$, distances to $\rho_0 = m_i v_{T0}/eB_0$, time to $\omega_{c0}^{-1} = m_i/eB_0$ and F to n_0/v_{T0}^3. Here, m_i is the ion mass and e the elementary charge. In equation (2), B is the normalized modulus of the dimensionless magnetic field $\mathbf{B} = (R_0/R)\mathbf{b}$, where $\mathbf{b}$ is the unit vector parallel to the magnetic field and R_0 the major radius on the magnetic axis. R is the major radius: $R = R_0 + r\cos\theta$, r being the minor radius and θ the poloidal angle. The electrostatic potential ϕ is normalized to the thermal energy (ϕ standing for $e\phi/T_0$). The subscript eq stands for equilibrium quantities, the brackets $\langle \cdot \rangle$ represent a flux-surface average, and n_i is the normalized ion guiding-center density.

The right-hand side of eq.(1) accounts for collisions $\mathcal{C}(F)$[15] and heat sources S. The source term is essential for the study of neoclassical and turbulent transports on energy confinement times, away from the initial state. The EGAM instability belongs to the more general class of bump-on-tail instabilities, where the drive comes from a positive slope of the distribution function in velocity space. Therefore, it is required to invert the negative slope of the initial Maxwellian distribution function so as to obtain an out-of-equilibrium state. The system will then tend to relax towards the thermodynamical equilibrium unless it is forced by additional external sources aiming at inverting continuously the population. To this end, the source S is made of two components: $S = S_{\text{th}} + S_{\text{EP}}$, with S_{th} a source of thermal energy[16] and S_{EP} an EP heating, hence leading to a positive slope in energy. S_{th} is localized in the inner region while S_{EP} is spread across the mid radial position $r_{\text{mid}} = (r_{\min} + r_{\max})/2$. The source S_{EP} is built by using projections onto Laguerre and Hermite polynomial basis, which enables a separation between injection of energy, parallel momentum and vorticity with a convenient choice of real coefficients[17]. The coefficients are chosen so as to inject only parallel energy. For symmetry reasons, the source is written as

$$S_{\text{EP}} = S_{\text{EP},0}(t)\, S_r(r)\, (S_+ + S_-)\, e^{-\bar{\mu}B(r,\theta)} \qquad (3)$$

where $S_{\text{EP},0}$ is the amplitude of the source and S_r its radial envelope ($\int r\, dr\, S_r = 1$). $\bar{\mu}$ stands for $\mu/T_{s\perp}$, with μ the adiabatic invariant and $T_{s\perp}$ the normalized transverse temperature of the source, set to 1 in the present simulations. $S_\pm$ includes the decomposition onto the specified polynomial basis

$$S_\pm = e^{-(\bar{v}_\parallel \pm \bar{v}_0)^2} \sum_{h,l} c_{hl} \mathcal{H}_h(\bar{v}_\parallel \pm \bar{v}_0)\, \mathcal{L}_l(\bar{\mu}B(r,\theta)) \qquad (4)$$

where $\mathcal{H}_h$ and $\mathcal{L}_l$ are the Hermite and Laguerre polynomials of degree h and l respectively. Here, $\bar{v}_0 = v_0/\sqrt{2T_{s\parallel}}$ is an arbitrary normalized velocity v_0 divided by the normalized parallel temperature of the source $T_{s\parallel}$, and $\bar{v}_\parallel$ stands for $\bar{v}_\parallel = v_\parallel/\sqrt{2T_{s\parallel}}$. Both v_0 and $T_{s\parallel}$ are critical parameters in view of exciting EGAMs (see below). This source mimics the effects of two tangential neutral beam injectors, oriented in the co- and counter-current directions so that no external momentum injection exists.

Two simulations are presented, characterized by the following dimensionless parameters: the collisionality is $\nu_\star = 0.02$ (banana regime), the profile of the safety factor q is parabolic with relatively low magnetic shear ($0 < r\, d_r \log q < 0.4$) and such that $q(r_{\text{mid}}) \approx 2.7$. The normalized Larmor radius is $\rho_\star = \rho_0/a = 1/150$ (with a the minor radius of the poloidal cross-section). The initial density and temperature profiles are characterized by $R_0/L_n = 2.2$ and $R_0/L_T = 6.5$ respectively, with where $L_{n,T} = -(d_r \log\{n,T\})^{-1}$ the density and temperature gradient lengths. L_n remains constant during the simulations. Both simulations are identical in the time window $0 < t < t_{\text{init}} = 2250$, where only the source S_{th} is used, with an input power of 4 MW. At t_{init}, turbulence has reached a statistically steady state. The source S_{EP} is then switched on, leading to an additional input power of 2 MW (beginning of phase A). In the following, the

two simulations are referred to as *simulation with EPs* ($v_0 = 2$, $T_{s\parallel} = 0.5$) and *simulation without EPs* ($v_0 = 0$, $T_{s\parallel} = 1$). In both simulations, the parallel and transverse injected energies are the same.

In the simulation with EPs, the source S_{EP} modifies the distribution function by depleting the population of particles around $v_\parallel \approx \pm v_0$ and creating two bumps on the tail of the distribution function. This modification leads to a reduction of ITG activity, which is explained as follows. Considering only resonant modes $k_\parallel = 0$, the resonance for ITG modes is $\omega - n\Omega_{dT}E = 0$, where n is the toroidal wave number, E the normalized kinetic energy and $\Omega_{dT} = \frac{q}{rR_0}\bar{\Omega}_d$ the normalized precession frequency, with $\bar{\Omega}_d$ a dimensionless frequency[18]. Following this simplified framework, the resonance occurs at $E = \mathrm{E}_\omega \equiv \omega/(n\Omega_{dT})$, which is estimated by considering that turbulence develops around the diamagnetic frequency $\omega_\star \approx k_\theta T/BL_n$[16], such that $\mathrm{E}_\omega \approx (T/\bar{\Omega}_d)R_0/L_n$ for resonant modes. Since the chosen value of R_0/L_n is close to $v_0^2/2$, the source S_{EP} leads to a reduction of the number of resonant particles for the ITG instability in this simulation. In the simulation *with EPs*, the depletion around E_ω occurs mainly in the outer region ($\rho > 0.5$). This is illustrated in figure 2a, where we plot the time evolution of the distribution function at $v_\parallel = v_0$ normalized to its value at $t = t_{\mathrm{init}}$. The observed reduction of turbulence for $\rho > 0.5$ (phase B of fig.1) then appears consistent with the linear stabilization of ITG modes due to this depletion mechanism.

In figure 2b we plot the time evolution of the slope of the distribution function at the resonant velocity $v_{\mathrm{res}} = q\omega_{EGAM}R$, with ω_{EGAM} the frequency of the EP mode[7,8,11]. After the introduction of S_{EP}, the slope is clearly inverted, mainly in the region $\rho > 0.5$. It is the positiveness of $\partial_{v_\parallel}F_{\mathrm{eq}}$ at the resonant velocity v_{res} in the simulation *with EPs* which drives EGAMs. This is evidenced by analyzing the contribution of the up-down poloidally asymmetric components, i.e. $\sin\theta$, to the axisymmetric modes, i.e. $n = 0$, of the electrostatic potential. The time Fourier transform of the imaginary part of the mode $\phi_{1,0}$ for $t > t_{\mathrm{init}}$ is shown in figure 3 for both simulations. We observe a peak at $\omega_{\mathrm{EGAM}} = 0.4\omega_{GAM}$ (and also the second harmonic at $2\omega_{\mathrm{EGAM}}$) which clearly dominates the spectrum in the simulation *with EPs* (solid red line). In the simulation *without EPs* (dotted blue line), the spectrum does not exhibit this peak. The imaginary part normalized to the modulus $|\phi_{1,0}|$ is also plotted (shadowed region) for the simulation *with EPs*. This curve clearly shows that the imaginary part dominates over the real part. Finally, analysis of the non axisymmetric modes proves that the EGAM frequency is embedded in the turbulence spectrum (not shown here). Therefore, analytical predictions of the effect of EGAMs on turbulence is not straightforward and the gyrokinetic simulations presented in this letter prove especially useful.
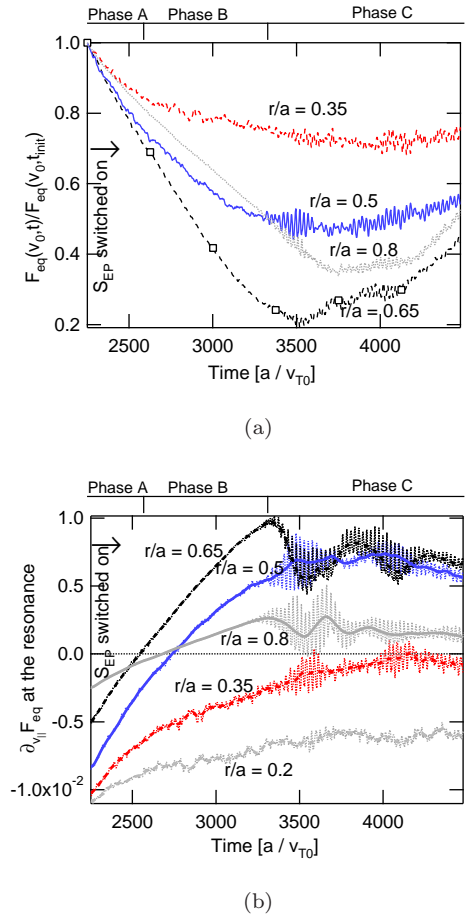

(a)

(b)

FIG. 2: Time evolution of the distribution function at $v_\parallel = v_0$ (top panel) and the derivative in velocity space at the EGAM resonant velocity (low panel).

An estimate of the $E \times B$ diffusivity is given by

$$\chi_{\mathrm{E}\times\mathrm{B}} \approx -\frac{Q_{E\times B}}{n_i\nabla_r T} \qquad (5)$$

where $Q_{E\times B} = \langle v_{Er}p \rangle$ is the radial heat flux associated to v_{Er} and p is the pressure. The time evolution of $\chi_{\mathrm{E}\times\mathrm{B}}$ is plotted in figure 4 for both simulations *with* (solid and dotted black lines) and *without* (dashed blue line) EPs in the region $0.5 < \rho < 0.8$. In the simulation *with EPs*, the expression 5 is decomposed into the contributions of axisymmetric and non axisymmetric modes. Three observations are made from this figure: (1) in the absence of EPs the modification of turbulent transport remains within the temporal fluctuations and is therefore not noticeable, (2) the contribution of axisymmetric modes in the simulation *with EPs* exhibits large amplitude oscillations around zero at the EGAM frequency, leading to a vanishing contribution when averaged over some EGAM cycles and (3) the $E \times B$ diffusivity, mainly due to non axisymmetric modes, increases during the EGAM activity in phase C and oscillates also at the EGAM frequency, indicating a strong interaction between turbulence and
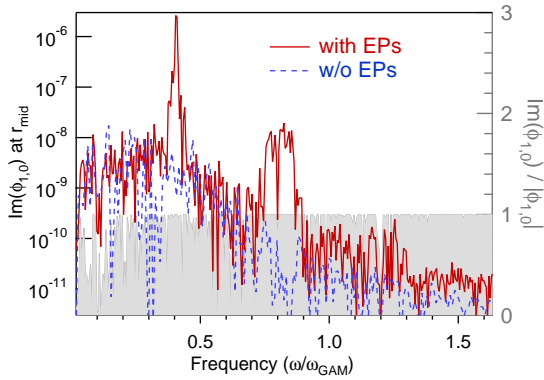
FIG. 3: Time Fourier transform of the $\sin\theta$ component of $\phi_{1,0}$ for both simulations *with* (solid red line) and *without* (dotted blue line) EPs. For the simulation *with EPs*, the imaginary part of $\phi_{1,0}/|\phi_{1,0}|$ is plotted (shadowed region).

EPs *via* EGAMs. As shown in figure 4, the increase of the $E \times B$ diffusivity is due to the non axisymmetric modes and represents therefore an increase of the turbulent transport triggered by the excitation of EGAMs.
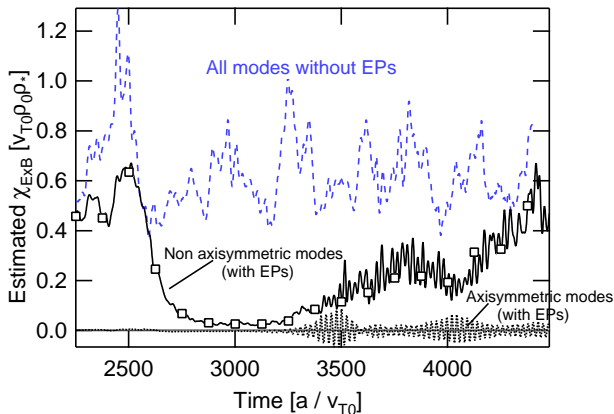

FIG. 4: Time evolution of the $E \times B$ diffusivity for both simulations. For the simulation *with EPs*, the respective contributions to $\chi_{E\times B}$ of axisymmetric modes (dotted black line) and of non-axisymmetric modes (solid black line) are distinguished. For the simulation *without EPs*, no distinction is made (dashed blue line).

The complex interaction between turbulence and EGAMs is captured in figure 5, where the evolution of the oscillating part of R_0/L_T is plotted at two different time windows. The oscillating part of R_0/L_T corresponds to $R_0/L_T - \langle R_0/L_T \rangle_t$, where $\langle \cdot \rangle_t$ is a time average. This figure corresponds to the first instants of the EGAM excitation at the end of the phase B (low panel) and to the phase where turbulence and EGAMs coexist, during phase C (top panel). During the transport barrier, the inner region exhibits avalanche-like behavior, as observed

in figure 5 (low panel), with fronts propagating outwards and vanishing at $\rho \approx 0.5$. The propagation velocity is of the order of $v_{aval} \approx 0.8 v_\star$, with $v_\star$ the ion diamagnetic velocity. In the same figure, we observe static oscillations in the outer region, characterized by horizontal traces. By *static* we mean that there is no front propagation, i.e. the beginning of the EGAM oscillations does not exhibit avalanche-like behavior for $\rho > 0.5$. However, in phase C (top panel of figure 5) we see that there is not a single propagation velocity, i.e. both outwards propagating fronts and static oscillations coexist and the outer radial region is also characterized by an avalanche-like behavior. This means that the inner avalanches propagate also in the outer region in the presence of EGAMs and the energy flows along the whole radial dimension by means of radially elongated structures. This result indicates in particular that a radial electric shear oscillating at a frequency $\omega \sim \omega_{turb}$ is likely not an efficient way to suppress turbulence.
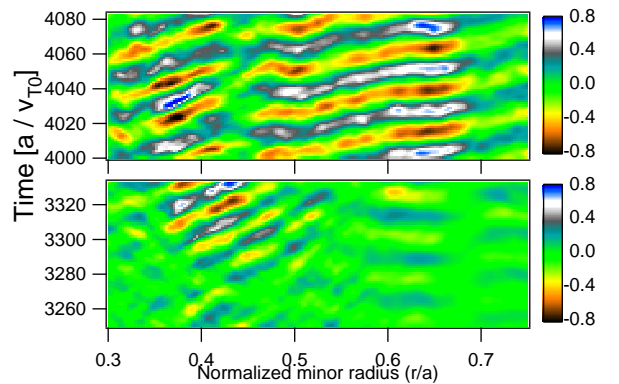

FIG. 5: Oscillating part of R_0/L_T in two time intervals of the *simulation with EPs*: end of phase B (bottom) and during phase C (top).

In conclusion, we have presented for the first time evidence of the modification of turbulence by energetic particles. This has been done in flux-driven gyrokinetic simulations, which represent a powerful tool in view of elucidating the complex interaction between turbulence and energetic particles *via* the excitation of EGAMs. We have shown that the presence of energetic particles in a transport barrier efficiently excites EGAMs, leading to an oscillating radial electric shear that does not suppress the turbulence. On the contrary, the effect on turbulent transport leads to the destruction of the pre-existing transport barrier. The complex interaction has been evidenced by the coupling between turbulence-driven avalanches and EGAM-driven static oscillations, resulting in a regime where turbulent transport (modulated at the EGAM frequency) and EGAMs coexist in steady state.

[1] P. Diamond, S. Itoh, K. Itoh, and T. Hahm, "Zonal flows in plasmas - a review," Plasma Physics and Controlled Fusion **47**, R35 (2005).

[2] E. Spiegel and J. Zahn, "The solar tachocline," Astronomy and Astrophysics **265**, 106–114 (1992).

[3] F. Busse, "Convection-driven zonal flows in the major planets," Pure and Applied Geophysics **121**, 375–390 (1983).

[4] W. Zhang, Z. Lin, and L. Chen, "Transport of energetic particles by microturbulence in magnetized plasmas," Phys. Rev. Lett. **101**, 095001 (2008).

[5] C. Holland, C. Petty, L. Schmitz, K. Burrell, G. McKee, T. Rhodes, and J. Candy, "Progress in gyro validation studies of diii-d h-mode plasmas," Nuclear Fusion **52**, 114007 (2012).

[6] N. Winsor, J. Johnson, and J. Dawson, "Geodesic acoustic waves in hydromagnetic systems," Physics of Fluids **11**, 2448 (1968).

[7] G. Fu, "Energetic-particle-induced geodesic acoustic mode," Physical review letters **101**, 185002 (2008).

[8] Z. Qiu, F. Zonca, and L. Chen, "Nonlocal theory of energetic-particle-induced geodesic acoustic mode," Plasma Physics and Controlled Fusion **52**, 095003 (2010).

[9] H. Berk, C. Boswell, D. Borba, A. Figueiredo, T. Johnson, M. Nave, S. Pinches, S. Sharapov, *et al.*, "Explanation of the jet n= 0 chirping mode," Nuclear fusion **46**, S888 (2006).

[10] R. Nazikian, G. Fu, M. Austin, H. Berk, R. Budny, N. Gorelenkov, W. Heidbrink, C. Holcomb, G. Kramer, G. McKee, *et al.*, "Intense geodesic acousticlike modes driven by suprathermal ions in a tokamak plasma," Physical review letters **101**, 185001 (2008).

[11] D. Zarzoso, X. Garbet, Y. Sarazin, R. Dumont, and V. Grandgirard, "Fully kinetic description of the linear excitation and nonlinear saturation of fast-ion-driven geodesic acoustic mode instability," Physics of Plasmas **19**, 022102–022102 (2012).

[12] V. Grandgirard, Y. Sarazin, X. Garbet, G. Dif-Pradalier, P. Ghendrih, N. Crouseilles, G. Latu, E. Sonnendrücker, N. Besse, and P. Bertrand, "Computing itg turbulence with a full-f semi-lagrangian code," Communications in Nonlinear Science and Numerical Simulation **13**, 81–87 (2008).

[13] K. Hallatschek and D. Biskamp, "Transport control by coherent zonal flows in the core/edge transitional regime," Physical Review Letters **86**, 1223–1226 (2001).

[14] G. Conway, C. Angioni, F. Ryter, P. Sauter, and J. Vicente, "Mean and oscillating plasma flows and turbulence interactions across the lh confinement transition," Physical Review Letters **106**, 65001 (2011).

[15] G. Dif-Pradalier, P. Diamond, V. Grandgirard, Y. Sarazin, J. Abiteboul, X. Garbet, P. Ghendrih, G. Latu, A. Strugarek, S. Ku, *et al.*, "Neoclassical physics in full distribution function gyrokinetics," Physics of Plasmas **18**, 062309 (2011).

[16] Y. Sarazin, V. Grandgirard, J. Abiteboul, S. Allfrey, X. Garbet, P. Ghendrih, G. Latu, A. Strugarek, and G. Dif-Pradalier, "Large scale dynamics in flux driven gyrokinetic turbulence," Nuclear Fusion **50**, 054004 (2010).

[17] Y. Sarazin, V. Grandgirard, J. Abiteboul, S. Allfrey, X. Garbet, P. Ghendrih, G. Latu, A. Strugarek, G. Dif-Pradalier, P. Diamond, *et al.*, "Predictions on heat transport and plasma rotation from global gyrokinetic simulations," Nuclear Fusion **51**, 103023 (2011).

[18] F. Zonca, P. Buratti, A. Cardinali, L. Chen, J.-Q. Dong, Y.-X. Long, A. Milovanov, F. Romanelli, P. Smeulders, L. Wang, Z.-T. Wang, C. Castaldo, R. Cesario, E. Giovannozzi, M. Marinucci, and V. P. Ridolfini, "Electron fishbones: theory and experimental evidence," Nuclear Fusion **47**, 1588 (2007).